Mechanisms of Ageing and Development 182 (2019) 111124

Contents lists available at ScienceDirect

Mechanisms of Ageing and Development

journal homepage: www.elsevier.com/locate/mechagedev

The synergistic action of phosphate and interleukin-6 enhances senescence-associated calcification in vascular smooth muscle cells depending on p53

Deping Xu[a,b,1], Fanjun Zeng[b,1], Linzi Han[b,c], Jun Wang[c], Zongzhi Yin[d], Liying Lv[a], Liyu Guo[b], Deguang Wang[c,*], Yuanhong Xu[a,*], Haisheng Zhou[b,e,*]

[a] Clinical Laboratory, The First Affiliated Hospital, Anhui Medical University (AHMU). No. 81 Meishan Rd., Hefei, China
[b] Department of Biochemistry & Molecular Biology, AHMU. No. 69 Meishan Rd., Hefei, China
[c] Department of Nephrology, The Second Affiliated Hospital, AHMU. No. 678 Furong Rd., Hefei, China
[d] Department of Obstetrics and Gynaecology, The First Affiliated Hospital, AHMU. No. 81 Meishan Rd., Hefei, China
[e] Center for Scientific Research, AHMU. No. 81 Meishan Rd., Hefei, China

ARTICLE INFO

Keywords:
IL-6
Phosphate
Senescence
Calcification
p53

ABSTRACT

Cardiovascular calcification is associated with cardiovascular morbidity and mortality of patients with end-stage renal diseases (ESRD). Hyperphosphatemia and many of the inflammatory markers and mediators, including interleukin-6 (IL-6), are considered as the major risk factors of cardiovascular calcification. Although cellular senescence may be involved in cardiovascular calcification caused by phosphate overload and (or) IL-6 in patients with ESRD, less is known about the underlying mechanisms for phosphate- and IL-6-induced senescence-associated calcification of vascular smooth muscle cells (VSMCs). In the present study, we investigated the correlation between cellular senescence and vascular calcification induced by loading phosphate and (or) IL-6 in VSMCs. Our findings show that p53 plays a major role in senescence-associated vascular calcification induced by phosphate overload. IL-6 induces senescence-associated calcification in VSMCs depending upon activation of the IL-6/soluble IL-6 receptor (sIL-6R)/signal transducer and activator of transcription 3 (STAT3)/p53/p21 pathway. We demonstrate that the synergistic action of phosphate overload and IL-6 enhances senescence-associated calcification in a p53-dependent manner and is inhibited by an anti-aging agent (resveratrol) in a dose-dependent manner.

1. Introduction

Cardiovascular calcification, including vascular and valvular calcification, is associated with cardiovascular morbidity and mortality of patients with end-stage renal diseases (ESRD) (Doulgerakis et al., 2017; Go et al., 2004a, b; London et al., 2003; O'Neill, 2016). Several observational studies have demonstrated that disturbed phosphate/calcium metabolism, osteogenic transition of vascular smooth muscle cells (VSMCs), senescent VSMCs, and VSMCs apoptosis are associated with cardiovascular calcification (Smith, 2016). Hyperphosphatemia, which is caused by indiscriminate phosphate/calcium metabolism, is a universal characteristic of patients with chronic kidney disease (CKD). As an independent cardiovascular risk factor, hyperphosphatemia has been linked to cardiovascular calcification in patients with ESRD (Hruska et al., 2008).

A proinflammatory state in patients with chronic uremia is considered as the other major risk factor of cardiovascular calcification. Many of the inflammatory markers and mediators, including interleukin-6 (IL-6), IL-1, tumor necrosis factor α (TNF-α), C-reactive protein, and fibroblast growth factor 23 (FGF23), are found to promote cardiovascular calcification in ESRD patients (Haydar et al., 2004; Isakova et al., 2018; Stompór et al., 2005; Stompor et al., 2004). Among

Abbreviations: ESRD, end-stage renal diseases; CKD, chronic kidney disease; NDD-CKD, non-dialysis-dependent chronic kidney disease; VSMCs, vascular smooth muscle cells; IL-6, interleukin-6; STAT3, signal transducer and activator of transcription 3; p-STAT3, phosphorlated-STAT3; SA-β-Gal, senescence-associated-β-galactosidase; L-Res, low concentrations of resveratrol; H-Res, high concentrations of resveratrol; α-SMA, α-smooth muscle actin; VEGFR2, vascular endothelial growth factor receptor 2; SIRT1, sirtuin 1; Ac-p53, acetylated-p53; ROS, reactive oxygen species

* Corresponding author at: (DG Wang) Department of Nephrology, The Second Affiliated Hospital, AHMU. No. 678 Furong Rd., Hefei, China; (YH Xu) Clinical Laboratory, The First Affiliated Hospital, Anhui Medical University (AHMU). No. 81 Meishan Rd., Hefei, China;(HS Zhou) Department of Biochemistry & Molecular Biology, AHMU. No. 69 Meishan Rd., Hefei, China.

E-mail addresses: wangdeguang@ahmu.edu.cn (D. Wang), xyhong1964@163.com (Y. Xu), haishengs@ahmu.edu.cn (H. Zhou).

[1] These authors are equal contribution to this work.

https://doi.org/10.1016/j.mad.2019.111124
Received 16 January 2019; Received in revised form 7 June 2019; Accepted 22 July 2019
Available online 01 August 2019

of these inflammatory factors, the elevated plasma IL-6 accelerates the progression of CKD not only by aggravating kidney injury, but also by initiating the chronic vascular disease, especially vascular calcification (Su et al., 2017). Results from *in vitro* studies and animal models of atherosclerosis suggest that IL-6 promotes vascular calcification in VSMCs (Alaly et al., 2007; Shioi et al., 2002; Yin et al., 2000). IL-6 in the vessel wall of conduit arteries likely induces adenine dinucleotide phosphate oxidase complex to produce reactive oxygen species, which mainly activates the signaling pathway depending upon signal transducer and activator of transcription 3 (STAT3) (Agharazii et al., 2015). This activation may contribute to vascular calcification in VSMCs in ESRD.

As an age-related kidney injury is consequent to reduction in glomerular filtration rate (GFR), decrease in urinary creatinine clearance, and reduced muscle mass, CKD is considered to be an age-related disease. Chronic stimulation of cells with cytokines causes enough stress to induce the cell senescence. Cellular senescence, also known as stress-induced premature senescence, is a state of the irreversible growth arrest of mitotic cells (Campisi and D'Adda, 2007) and leads to a decreased capacity to respond to various stimuli. An increased activity of senescence-associated-β-galactosidase (SA-β-Gal) is available, and a different series of genes, such as retinoblastoma protein, p21, p53, and p16, is expressed in senescent cells (Ben-Porath and Weinberg, 2005). Cellular senescence is involved in vascular calcification that contributes to the high cardiovascular mortality in CKD. *in vitro* studies have reported that senescence of VSMCs promotes vascular calcification (Nakano-Kurimoto et al., 2009; Yamada et al., 2015).

IL-6 and the soluble IL-6 receptor (sIL6R) are involved in the pathogenesis of tissue senescence (Hirano et al., 2000). IL-6 and sIL-6R induce premature senescence in normal human fibroblasts in a STAT3/p53-dependent manner (Kojima et al., 2012). On the other hand, several previous studies have proven that hyperphosphate is mainly responsible for the senescence-like phenotype, implying a potential relationship between phosphate and senescence. For example, FGF-23, which is secreted from bone, exerts the kidney to promote phosphaturia (Quarles, 2008). Klotho, as an aging-suppressor gene, is expressed predominantly in the renal tubular cells (Kuroo et al., 1997). Both hyperphosphatemia and senescence-like phenotype are observed in FGF-23-deficient mice and klotho-deficient mice (Kurosu et al., 2005; Razzaque et al., 2006).

However, the underlying mechanisms for phosphate-induced and IL-6-induced senescence-associated vascular calcification of VSMCs remain unclear. In this study, we investigated the correlation between cellular senescence and vascular calcification induced by phosphate and IL-6 in VSMCs. Phosphate overload-induced senescence-associated calcification upregulates p53 expression in VSMCs. Importantly, IL-6 induces senescence-associated calcification in VSMCs depending upon activation of the IL-6/sIL-6R/STAT3/p53/p21 signaling pathway. We show that the synergistic action of phosphate and IL-6 enhances senescence-associated calcification in a p53-dependent manner, and is inhibited by anti-aging agents in a dose-dependent manner.

2. Materials and methods

2.1. Patients

Selected cases of patients with ESRD were defined as estimated-glomerular filtration rate (eGFR) < 15 ml/min/1.73m^2 or albuminuria ≥ 300.0 mg/d. Patients with NDD-CKD were defined as eGFR < 60 ml/min/1.73m^2 for more than 3 months. Fasting plasma samples (phosphate > 1.45 mM, IL-6 > 5.59 pg/ml) and clinical data from patients with NDD-CKD (n = 38) and ESRD (n = 159) were collected at the Department of Nephrology in the Second Affiliated Hospital of AHMU. Among the patients with ESRD, 144 cases of patients were diagnosed using clinical images of vascular and valvular calcification obtained with plain X-rays or Doppler ultrasound imaging. Informed consent for experiments was not required because Chinese laws treat human tissues and plasma left from surgery or clinical examination as discarded materials.

2.2. Cell cultures and treatments

Human endothelial cells (EAhy926) were cultured in DMEM with 10% fetal bovine serum (FBS, Gibco BRL. NY, USA) and 1% penicillin/streptomycin (P/S). Primary human VSMCs isolated from the segments of umbilical artery and primary human skin fibroblasts were cultured in F12/DME medium with 20% FBS and 1% P/S. VSMCs were cultured to 80% confluence before passage. To induce vascular calcification and senescence, 5-passage VSMCs were treated for 1–5 days with a high level of phosphate (3.8 mM) or 50 ng/ml recombinant human IL-6 (eBioscience. San Diego, CA, USA). To ensure removal of spontaneous senescence, 5-passage VSMCs cultured in complete F12/DME medium with phosphate-buffered saline (PBS) for 5 days were used as the vehicle cells (5-day vehicle). Low concentrations of resveratrol (L-Res, 0.1 mg/ml) or high concentrations of resveratrol (H-Res, 0.2 mg/ml) were supplemented to attenuate senescence of VSMCs. Either 50 ng/ml anti-IL-6 neutralization antibody (Sino Biological, Beijing, China) or 20 μM pifithrin-α (PFTα, MedChemExpress, New Jersey, USA) was used to block IL-6 activities or to inhibit p53 functions.

2.3. Fluorescence immunocytochemistry

As described elsewhere (Tu et al., 2018), fluorescence immunocytochemistry was used to detect expression of α-SMA, vimentin, and VEGFR2 in VSMCs with the rabbit anti-α-SMA antibody (1:200 dilution; Bioss, Beijing, China), the rabbit anti-vimentin antibody (1:100 dilution, CST, USA), and the rabbit anti-VEGFR2 antibody (1:400 dilution, Affinity Biosciences, USA), respectively.

2.4. Western blotting

A total 40 μg of total proteins were used to run SDS-PAGE and then to perform Western blotting analysis. Western blotting was performed as previously described (Zhao et al., 2016). The primary antibodies include SIRT1 (1:1000 dilution, CST), p53 (1:1000 dilution, CST), acetylated-p53 (Ac-p53, Lys382. 1:2000 dilution, Abcam), STAT3 (1:1000 dilution, CST), phosphorlated-STAT3 (p-STAT. 1:2000 dilution, CST), p21 (1:1000 dilution, CST), and glyceraldehyde 3-phosphate dehydrogenase (GAPDH) (1:5000 dilution, IMAGEN, Beijing, China). Western blotting bands were captured by using the development instrument from Shanghai Qinxiang Scientific Instrument Co. LTD. The relative protein quantification analysis was performed by using Image J software.

2.5. Determination of calcification

For quantification of Calcium deposition, VSMCs were decalcified with 0.6 N HCl for 24 h, and the calcium content in the supernatant was detected with the total protein quantitative test kit and a calcium ion test kit (Jiancheng Bioengineering Institute, Nanjing, China), according to the manufacturer's introductions.

Alizarin Red S staining was used to detect mineral deposition of VSMCs. The samples were fixed with 4% paraformaldehyde for 20 min, stained for 5 min with 1% Alizarin Red S staining solution (pH 4.2), and rinsed with distilled water. The calcification of cells was detected by a calcium salt dyeing liquid kit (Solarbio, Beijing, China).

2.6. SA-β-Gal staining

SA-β-Gal staining was used to assess the senescent state in VSMCs with a β-galactosidase senescence staining kit (Beyotime Biotechnology), according to the manufacturer's introductions. In brief,

cells were fixed with 4% paraformaldehyde for 20 min, washed, and incubated at 37℃ overnight in staining solution.

2.7. Measurement of intracellular levels of reactive oxygen species (ROS)

Intracellular ROS was measured by using ROS assay kit (Solarbio) according to the manufacturer's protocols. In brief, VSMCs were incubated with 2′7′-dichlorodihydrofluorescein diacetate (DCFH-DA) at 37 ˚C for 20 min, harvested, washed with PBS, and then detected immediately by flow cytometry. An increase in fluorescence intensity was used to quantify the generation of net intracellular ROS.

2.8. Luciferase assays

Transcriptional activity was referenced as described elsewhere. (Zhao et al., 2016) Briefly, the 293 T cells were transiently transfected with pGL3-basic vectors (Promega, Madison, WI, USA) containing human wild-type *p53* promoter or a mutated *p53* promoter. Renilla (pRL-TK) luciferase plasmids were used as the controls. After transfected for 12 h, cells were treated with 30 ng/ml IL-6 for 24 h. Then, luciferase assays were performed to detect relative activities of human *p53* promoters.

2.9. Statistical analysis

All values are expressed as the mean ± SD. Statistical analyses were performed using analysis of variance (ANOVA) followed by the one-way ANOVA test and the Nonparametric test. Differences with a P value of < 0.05 were considered to be statistically significant.

3. Results

3.1. Hyperphosphatemia and high levels of serum IL-6 are complicated with vascular calcification in patients with ESRD

Serum determinations of inorganic phosphate and IL-6 from patients with ESRD and non-dialysis-dependent chronic kidney disease (NDD-CKD) were collected in the present study. Data showed that serum inorganic phosphate was 1.63 ± 0.58 mM, and serum IL-6 was 21.32 ± 38.68 pg/ml in 159 cases of patients with ESRD. Serum inorganic phosphate and IL-6 was 1.28 ± 0.31 mM and 12.37 ± 31.00 pg/ml in 38 cases of patients with NDD-CKD, respectively. The non-parametric tests showed significant differences in the levels of serum inorganic phosphate ($P < 0.001$) and IL-6 ($P = 0.0018$) between the ESRD group and the NDD-CKD group (Fig. 1A, 1B).

To study the correlations between calcification and high levels of inorganic phosphate as well as serum IL-6, the clinical cardiovascular calcification images, including vascular calcification and valvular calcification, were collected from 144 cases of ESRD patients with serum determinations of both phosphate and IL-6. The plain X-rays and Doppler ultrasound imaging showed that cardiovascular calcification was found in 60 patients with ESRD (41.67%, 60/144), whereas 58.33% of patients had no calcification (84/144) (Fig. 1C). As shown in Fig. 1D and Table 1, both high phosphate and elevated serum IL-6 were found in 45.00% of ESRD patients with cardiovascular calcification (27/60). High phosphate was found in 15.00% of patients (9/60), and 25.00% patients had higher serum IL-6 levels (15/60). For 84 cases of patients without calcification, there were 17.86% (15/84), 23.81% (20/84), and 34.52% (29/84) of patients with high phosphate, with high serum IL-6, and with both, respectively. The cross-table chi-squared test showed that cardiovascular calcification is correlated with high levels of phosphate and elevated serum IL-6 level in patients with ESRD ($P = 0.00$).

3.2. Either phosphate or IL-6 induces senescence-associated vascular calcification in VSMCs

To investigate whether phosphate overload induces senescence-associated vascular calcification, primary human VSMCs were isolated from the segments of umbilical artery and used as a cell model in our experiments. Alpha-SMA, as a specific marker of VSMCs, was successfully detected both in primary VSMCs and the 5th passage VSMCs by fluorescence immunocytochemistry analysis with an anti-α-smooth muscle actin (α-SMA) antibody, whereas vimentin (a molecular marker of fibroblasts) as well as VEGFR2 (a specific marker of endothelial cells) were not shown in VSMCs (Fig. 2A). To ensure removal of spontaneous senescence, 5-day-cultured cells in complete F12/DME medium with phosphate-buffered saline (PBS) were used as the control cells (5-day vehicle). As shown in Fig. 2B, expression of p21 was dramatically increased in VSMCs treated with a high level of phosphate (3.8 mM) for 3 to 5 days. However, the increased expression of p21 in VSMCs was inhibited after treatment by low levels of resveratrol (0.1 mg/ml resveratrol, L-Res). SA-β-Gal expression is the other key feature of senescence in many cell types when they undergo senescence because of multiple stimuli. SA-β-Gal staining analysis showed that phosphate treatment generated a dramatic increase SA-β-Gal expression in VSMCs, whereas the SA-β-Gal activity was not significantly altered in VSMCs by exposure to L-Res over 5 days of phosphate overload (Fig. 2C). Additionally, ROS, as the cellular biomolecules of senescence, leads to the decline of physiological functions. The ROS levels in VSMCs treated with loading phosphate were increased 1.2–1.8 folds than those in the 5-day-cultured cells. But L-Res could decrease ROS levels in VSMCs by exposure to phosphate overload for 2–5 days (Fig. 2D).

Calcification levels were determined on the basis of calcium content and Alizarin Red S staining to further examine degree of calcification of VSMCs. The calcium content in VSMCs treated with loading phosphate was markedly increased compared with 5-day-cultured cells. On the contrary, the increased calcium content in VSMCs was dramatically inhibited after treatment by L-Res (Fig. 2E). Furthermore, Alizarin Red S staining showed that phosphate overload also markedly enhanced mineral deposition in VSMCs, and that phosphate-induced calcification of VSMCs was dramatically attenuated when VSMCs were treated with L-Res for 1–5 days (Fig. 2F). Taken together, these results indicate that phosphate overload has a role in inducing senescence-associated vascular calcification.

Given that IL-6 may have a role in inducing senescence-associated vascular calcification, expression of SA-β-Gal and p21 in VSMCs exposed to IL-6 was detected using SA-β-Gal staining assay and western blotting analysis, respectively. As shown in Fig. 3A and B, SA-β-Gal as well as p21 were markedly increased in VSMCs exposed to IL-6 by days 3 and 5. An increased expression of SA-β-Gal and p21 was dramatically inhibited when VSMCs were treated by L-Res for 5 days. The ROS levels in VSMCs treated with IL-6 were increased 1.4–1.8 folds than those in the 5-day-cultured cells. But L-Res could significantly decrease ROS levels in VSMCs by exposure to IL-6 for 2–5 days (Fig. 3C). Similar to phosphate-induced senescence-associated vascular calcification, IL-6 enhanced mineral deposition in VSMCs, and L-Res treatments prevented vascular calcification from IL-6 induction of VSMCs over 5 days according to Alizarin Red S staining and calcium content (Fig. 3D and E).

3.3. Either phosphate overload or IL-6 induces senescent VSMCs in a p53-dependent manner

To investigate the underlying mechanisms of phosphate-induced and IL-6-induced senescence-associated vascular calcification of VSMCs, we firstly determined sirtuin 1 (SIRT1) expression in VSMCs induced by phosphate overload or IL-6. As expected, immunoblotting results showed p21 expression dramatically increased consistent with a low level of SIRT1 expression in VSMCs treated with phosphate

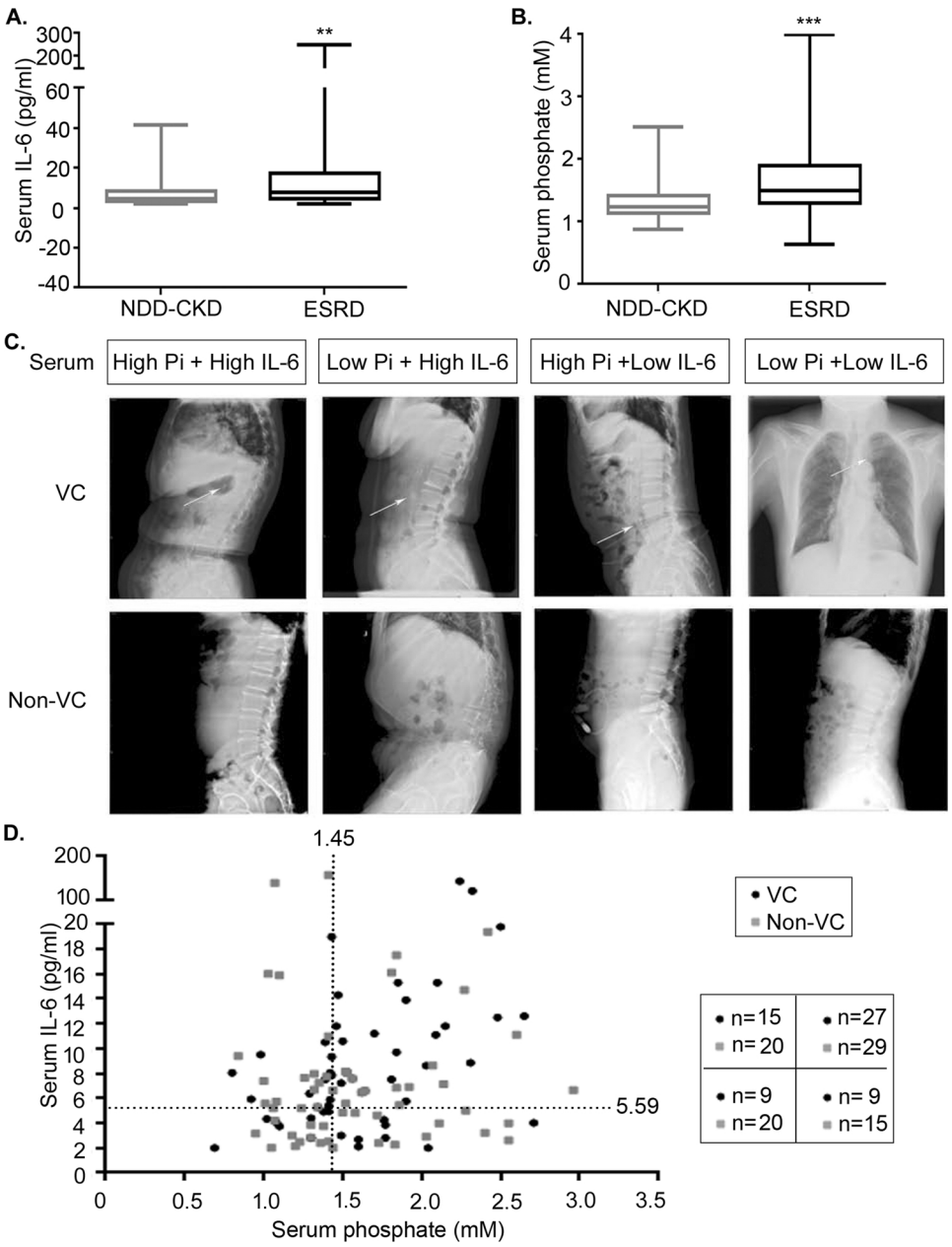

Fig. 1. Cardiovascular calcification is coincident with high serum levels of IL-6 and phosphate in patients with ESRD compared to those in patients with NDD-CKD. A, B. Serum levels of IL-6 and phosphate in patients with ESRD and NDD-CKD. Bottom, middle, and top lines of each box correspond to the 25th, 50th, and 75th percentiles, respectively. $^{**}P < 0.01$, $^{***}P < 0.001$ versus NDD-CKD group. C. Plain X-rays images of vascular calcification in patients with ESRD. In VC groups, the strip-shaped or curved high-density shadow can be clearly found along the abdominal aorta areas or in the aortic node. However, calcification was negative in X-ray images in non-VC groups. Arrows denote the high-density shadows (calcification sites). D. Comparison of serum levels of IL-6 and phosphate in patients with ESRD. Pi, serum phosphate. VC, ESRD patients with calcification; Non-VC, ESRD patients without calcification.

Table 1
Summary of serum phosphate, IL-6 and calcification states of patients with ESRD.

Serum	Calcification Images		Total (cases)
	Yes	No	
Pi[a] ↑[b] + IL-6 ↑	27	29	56
Pi ↑ + IL-6 ↓[c]	9	15	24
Pi ↓ + IL-6 ↑	15	20	35
Pi ↓ + IL-6 ↓	9	20	29
Total (cases)	60	84	144

[a] Pi, serum phosphate.
[b] Up arrow, high levels of serum phosphate (> 1.45 mM) or IL-6 (≥ 5.59 pg/ml).
[c] Down arrow, low levels of serum phosphate (≤ 1.45 mM) or IL-6 (< 5.59 pg/ml).

overload or IL-6 for 3–5 days (Fig. 4A), according to the time-course expression analysis (Fig. 4B), loading either phosphate-induced or IL-6-induced senescent VSMCs generated the same expression patterns of p53 coincident with those of p21 since the IL-6/sIL-6R signaling pathway usually activates STAT3 and induces expression of the target genes. Not surprisingly, we found that activated-STAT3 (p-STAT3) was markedly increased in senescent VSMCs induced by IL-6, whereas p-STAT3 showed no significant alternations in VSMCs by exposure to loading phosphate alone.

To confirm whether IL-6-induced p-STAT3 regulates *p53* expression, a reporter construct containing the luciferase gene under the control of the −1998 to -1514 bp fragment from the human *p53* gene locus (chr: 17p13.1) was transfected into 293 T cells. Relative luciferase activities were significantly increased in 293 T cells by exposure to IL-6 (Fig. 4C). Furthermore, within this region is a consensus sequence 5′-TTnnnnGAA-3′ (-1761 bp) previously described as the potential p-STAT3 binding site (Tu et al., 2018). After deleting the specific binding site, human *p53* promoter had not responses to IL-6. The data prompt us to conclude that p53 expression is regulated by activating IL-6/sIL-6R/

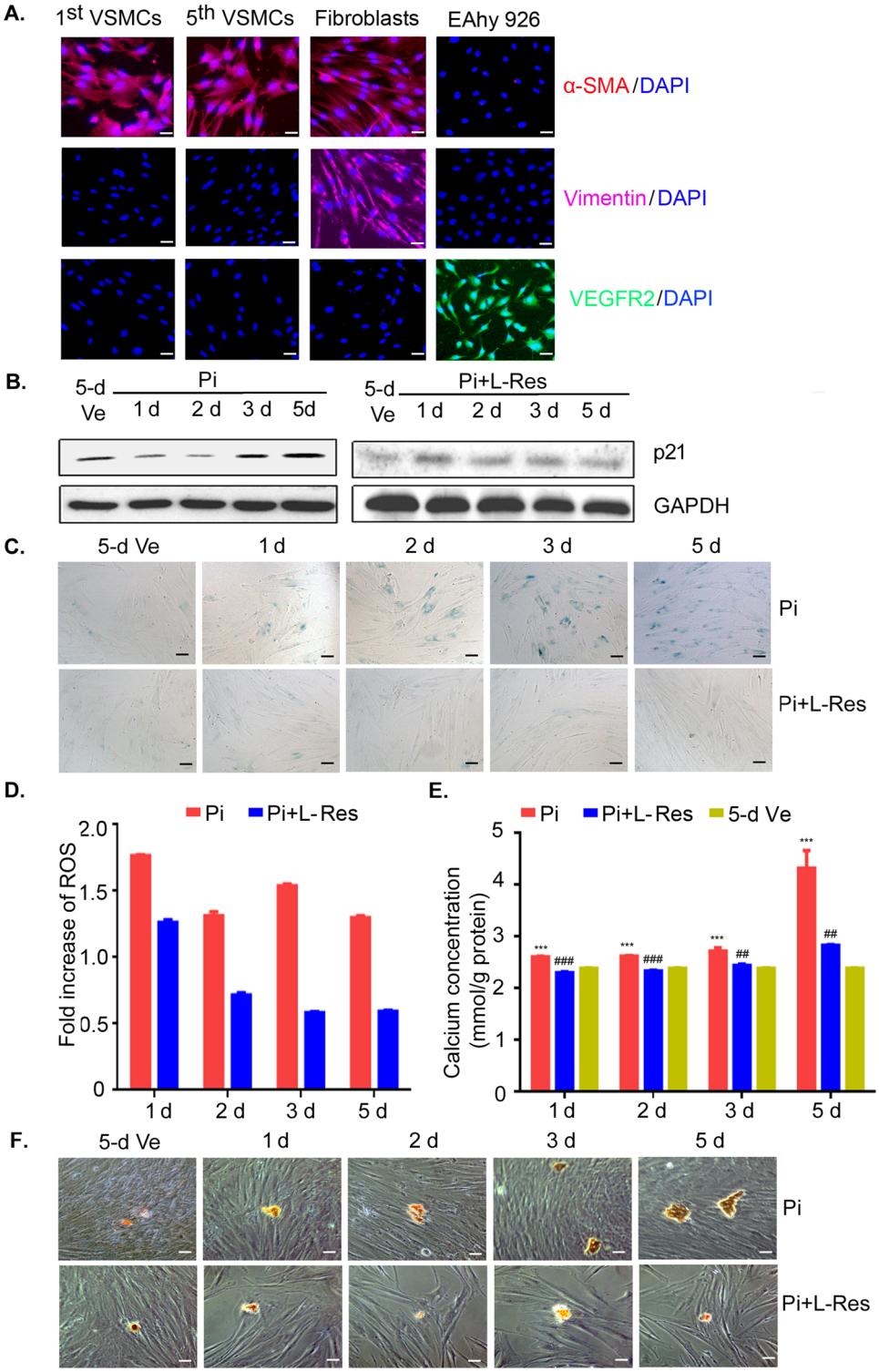

Fig. 2. Phosphate overload induces senescence-associated calcification in VSMCs. A. Fluorescence immunocytochemistry analysis for α-SMA, vimentin and VEGFR2 expression in VSMCs, human primary fibroblasts and EAhy926 cells. The 1st and 5th VSMCs, the primary VSMCs and the 5th passages of VSMCs. Scale bar = 100 μm. B. Immunoblotting analysis for the detection of p21 expression in VSMCs by exposure to phosphate alone (Left), as well as phosphate and low levels of resveratrol (L-Res, Right). C. SA-β-Gal staining to determine the senescent VSMCs exposed to loading phosphate alone (Top), both phosphate overload and L-Res (Bottom). Scale bar = 50 μm. D. ROS levels of VSMCs stimulated by loading phosphate alone, or by phosphate overload as well as L-Res. The Y-axis denotes folds increase of the fluorescence intensity (ROS) comparing to the value of 5-day vehicle. E. Calcium content in the supernatant of VSMCs compared with total proteins in VSMCs. Data were presented as the mean ± SD of triplicate experiments (***$P < 0.001$ versus 5-day vehicle; ##$P < 0.01$, ###$P < 0.001$ versus phosphate overload). F. Alizarin red staining for detection mineral deposition in VSMCs in presence of loading phosphate alone (Top) or both phosphate overload and L-Res (Bottom). Scale bar = 50 μm. Pi, 3.8 mM phosphate; L-Res, 0.1 mg/ml resveratrol; 5-d Ve (5-day vehicle) means VSMCs cultured in medium without stimuli for 5 days.

STAT3/p53 pathway.

As resveratrol mainly depends upon upregulation of SIRT1 to attenuate cellular senescence, immunoblotting showed that L-Res dramatically increased SIRT1 expression in VSMCs exposed to either phosphate overload or IL-6 alone, coincident with a decreased p21 expression (Fig. 4D). Furthermore, in accordance with an increased SIRT1 expression induced by resveratrol, a decrease in Ac-p53 was observed in VSMCs in the presence of either loading phosphate or IL-6. Meanwhile, compared with 5-day vehicle, p53 expression showed no significant alteration. It is suggested that either phosphate overload or IL-6 induces senescent VSMCs in a p53-dependent manner.

3.4. The synergistic action of phosphate and IL-6 enhances senescence-associated calcification

Because both hyperphosphatemia and high levels of serum IL-6 usually occur in patients with ESRD, VSMCs were stimulated with both phosphate overload and IL-6 to investigate their synergistic actions in inducing senescence-associated vascular calcification. As shown in Fig. 5A, p21 expression was markedly increased in VSMCs treated with

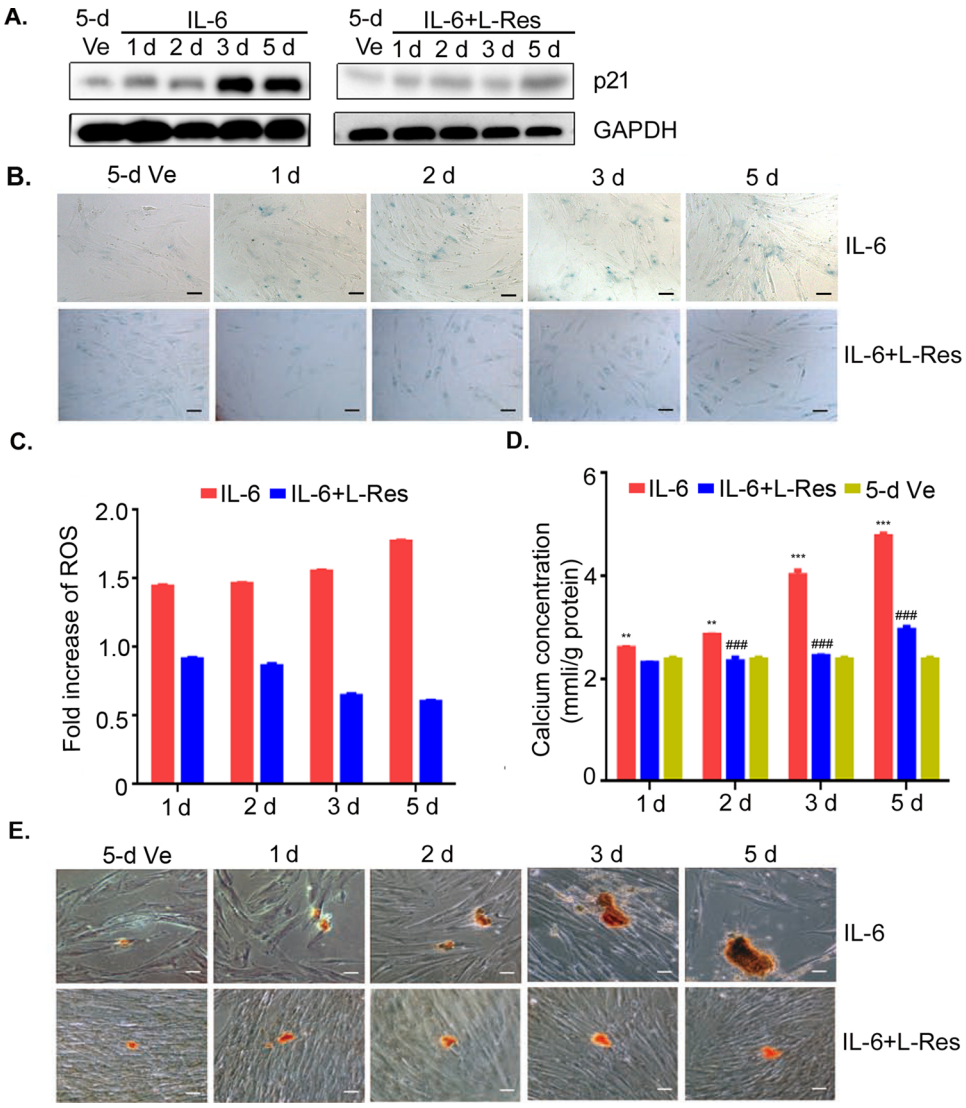

Fig. 3. IL-6 induces senescence-associated calcification in VSMCs. A. Immunoblotting analysis for the detection of p21 expression in VSMCs by exposure to IL-6 (Left), IL-6 and resveratrol (L-Res, Right). B. SA-β-Gal staining for determining the senescent VSMCs exposed to IL-6 alone (Top) and both IL-6 and L-Res (Bottom). Scale bar = 50 μm. C. ROS levels of VSMCs stimulated by IL-6 alone, or by IL-6 as well as L-Res. The Y-axis denotes folds increase of the fluorescence intensity (ROS) comparing to the value of 5-day vehicle. D. Calcium content in the supernatant of VSMCs compared with total proteins in VSMCs. Data were presented as the mean ± SD of triplicate experiments ($^{**}P < 0.01$, $^{***}P < 0.001$ versus 5-day vehicle; $^{\#\#\#}P < 0.001$ versus IL-6 treatment). VSMCs were treated for 1–5 days by IL-6 alone, or by IL-6 as well as L-Res. E. Alizarin red staining for detection of mineral deposition in VSMCs in the presence of IL-6 alone (Top) or both IL-6 and L-Res (Bottom). Scale bar = 50 μm. Five-day vehicle represents VSMCs cultured in growth medium without stimuli for 5 days.

both phosphate overload and IL-6 by 1 day. Unexpectedly, L-Res did not inhibit an increase p21 expression in VSMCs exposed to both phosphate overload and IL-6, whereas, a high level of resveratrol (H-Res, 0.2 mg/ml) effectively inhibited the increased expression of p21 in VSMCs. SA-β-Gal staining assay exhibited that the combined action of phosphate and IL-6 enhanced SA-β-Gal expression in VSMCs (Fig. 5B, top). Furthermore, an increased activity of SA-β-Gal was still observed in VSMCs by exposure to L-Res by 5 days (Fig. 5B, middle). However, in response to H-Res, SA-β-Gal activities induced by the combined action of phosphate and IL-6 were markedly weakened (Fig. 5B, bottom). The ROS levels in VSMCs exposed to both phosphate overload and IL-6 were markedly increased compared with those in the 5-day-cultured cells, and this effect was significantly attenuated in the presence of L-Res or H-Res (Fig. 5C).

For quantification of calcium deposition, the calcium content in VSMCs treated with loading phosphate and IL-6 was markedly increased compared with 5-day-cultured cells. On the contrary, the increased calcium content in VSMCs was dramatically inhibited after treatment for 3–5 days by H-Res instead of L-Res (Fig. 5D). Furthermore, Alizarin Red S staining showed that mineral deposition was dramatically increased in VSMCs by exposure to phosphate overload and IL-6 for 1–5 days (Fig. 5E, top). Although calcification of VSMCs was inhibited when VSMCs were exposed to L-Res for 1–3 days, mineral deposition was still increased by exposure to L-Res by 5 days (Fig. 5E, middle). H-Res dramatically inhibited mineral deposition in VSMCs induced by the combined action of phosphate and IL-6 for 1–5 days (Fig. 5E, bottom). Additionally, a significantly increased calcium deposition was still observed when VSMCs were exposed to L-Res by 5 days. However, H-Res dramatically decreased the calcium concentration of VSMCs over 5 days. It has been suggested that the combined action of phosphate and IL-6 in inducing senescence-associated vascular calcification is inhibited by resveratrol in a dose-dependent manner.

To further investigate the underlying mechanisms for the synergistic actions of phosphate overload and IL-6 inducing senescence-associated vascular calcification, immunoblotting analysis was performed to determine SIRT1, p21, p53, and p-STAT3 in VSMCs by exposure to both phosphate overload and IL-6. Similar to the increase expression of p21 by 1-day-induction, an increasing expression of p53 and activation STAT3 (p-STAT3) was observed in VSMCs by exposure to both phosphate overload and IL-6, while SIRT1 was expressed at a low level (Fig. 6A). In response to L-Res, a dramatically increased expression of SIRT1 was observed in VSMCs treated with both loading phosphate and IL-6 only by 3 and 5 days (Fig. 6B). Unexpectedly, an increasing expression of p53 and Ac-p53 was still observed in VSMCs in the presence of loading phosphate, IL-6, and L-Res by 3 and 5 days, coincident with the increase expression of p21. However, when VSMCs were treated with H-Res, SIRT1 expression markedly increased by 2 days and maintained high levels over 3–5 days. Coincident with an increase in

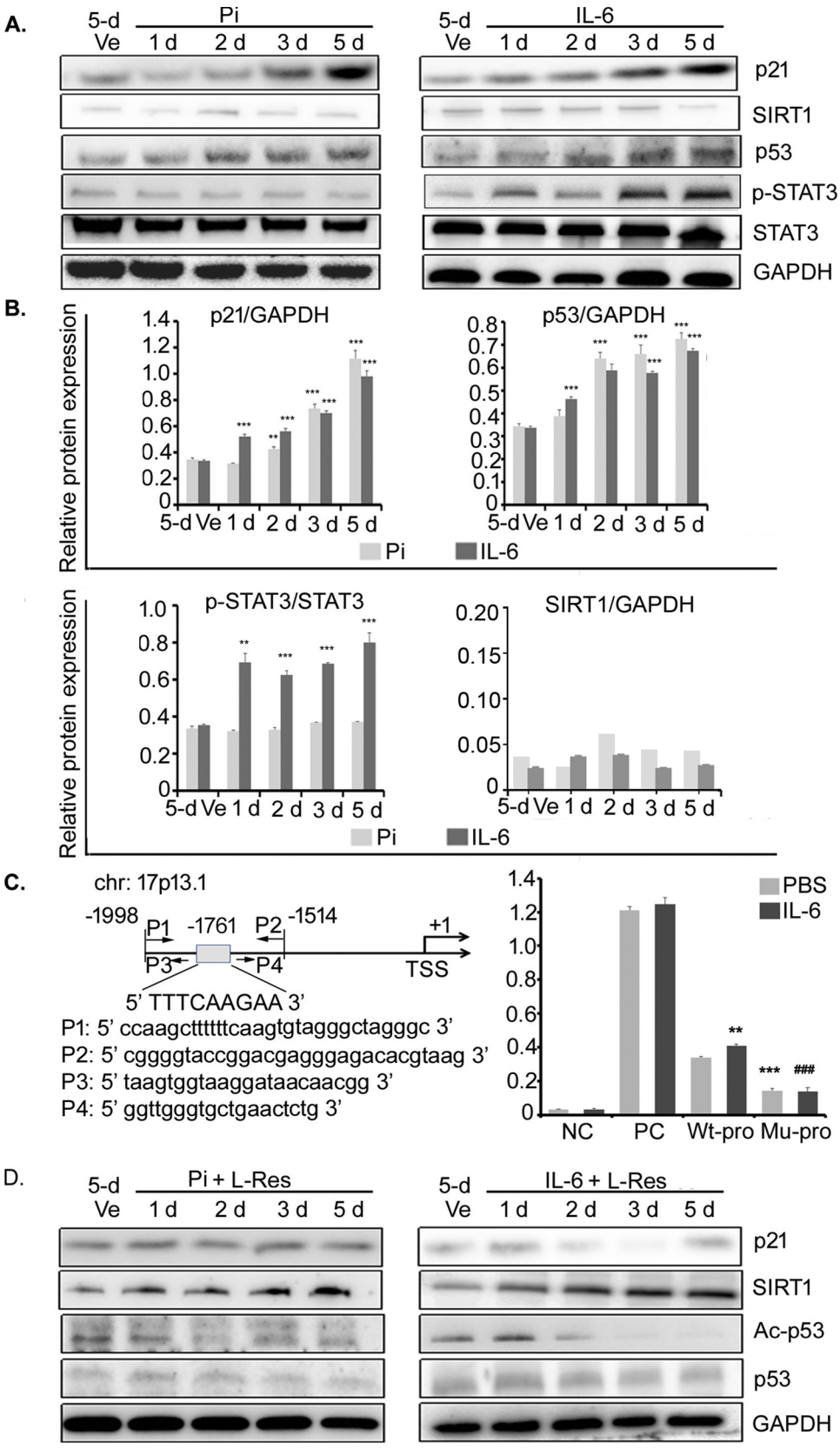

Fig. 4. Either phosphate overload or IL-6 induces VSMCs senescence in a p53-dependent manner. A. Western blotting analysis for the detection of p21, SIRT1, p53, STAT3, and p-STAT3 in VSMCs exposed to 3.8 mM phosphate (Pi) or 50 ng/ml IL-6 for 1 to 5 days. 5-d Ve (5-day vehicle) denotes VSMCs cultured in growth medium without stimuli for 5 days. B. Relative protein expression of p21, p53, p-STAT3, SIRT1 of VSMCs exposed to phosphate and IL-6 for 1 to 5 days. Data were presented as the mean ± SD of triplicate experiments ($^{**}P < 0.01$, $^{***}P < 0.001$ versus 5-day vehicle). C. Luciferase analysis for activities of human *p53* promoter induced by IL-6 (30 ng/ml). The potential *p53* promoter fragment (-1998-1514 bp) was obtained from human genomic DNA of VSMCs using polymerase chain reaction (PCR) with the primer 1 and 2 (P1 and P2), and cloned into the pGL3 basic vector with *KpnI* and *HindIII*. The potential p-STAT3 binding sequences of 5′-TTTCAA GAA-3′at -1761 bp were deleted by using specific PCR with the primer 3 and 4 (P3 and P4). TSS, transcriptional start site. NC, negative control. PC, positive control. Wt-pro, wild type promoter of *p53*. Mu-pro, mutated promoter of *p53*. Data were presented as the mean ± SD of triplicate experiments ($^{**}P < 0.01$, $^{***}P < 0.001$ versus wild type promoter of *p53* treated with PBS; $^{\#\#\#}P < 0.001$ versus wild type promoter of *p53* treated with IL-6). D. Immunoblotting analysis for detection of p21, SIRT1, p53, and Ac-p53 in VSMCs by exposure to L-Res with 3.8 mM phosphate (Pi, Left) or IL-6 (Right) for 1 to 5 days. 5-d Ve (5-day vehicle) denotes VSMCs cultured in growth medium without stimuli for 5 days.

SIRT1 expression, p53 and Ac-p53 dramatically decreased, and there were no significant alterations of p21 expression. Therefore, senescence-associated calcification of VSMCs could be inhibited by resveratrol in a dose-dependent manner.

To further examine whether blocking IL-6/STAT3/p53/p21 signal pathway might lead to inhibiting senescence-associated calcification of VSMCs, VSMCs were treated for 1–5 days with an anti-IL-6 neutralization antibody. Immunoblotting analysis showed the levels of p-

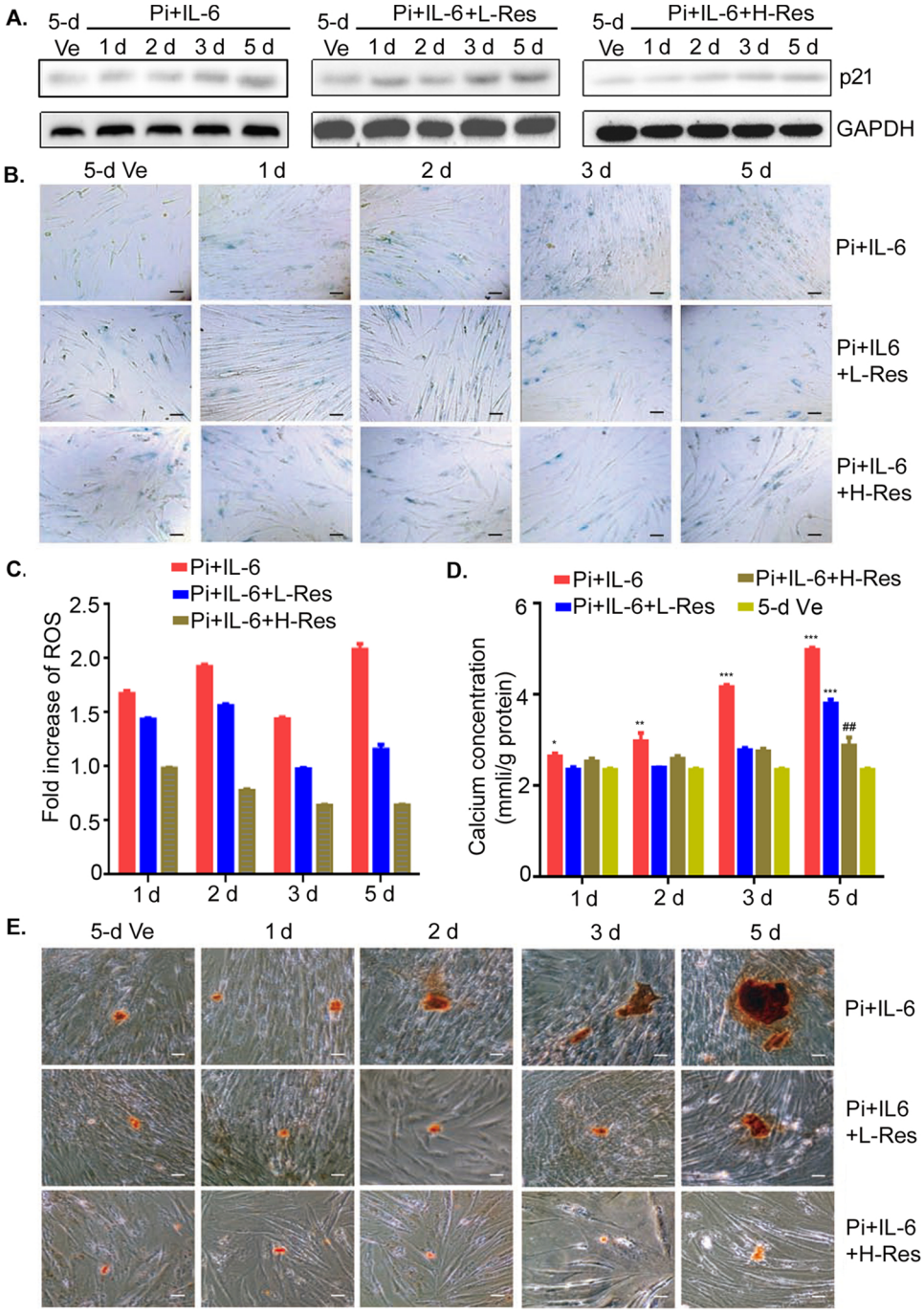

Fig. 5. The synergistic action of phosphate and IL-6 enhances senescence-associated calcification. A. Immunoblotting analysis for detection of p21 expression in VSMCs. B. SA-β-Gal staining for determining the senescent VSMCs (Scale bar = 50 μm). C. Either L-Res or H-Res decreased ROS levels of VSMCs by exposure to both phosphate and IL-6. The Y-axis denotes folds increase of the fluorescence intensity (ROS) comparing to the value of 5-day vehicle. D. Calcium content in the supernatant of VSMCs compared with total proteins in VSMCs. Data were presented as the mean ± SD of triplicate experiments ($^{*}P < 0.05$, $^{**}P < 0.01$, $^{***}P < 0.001$ versus 5-day vehicle; $^{\#\#}P < 0.01$ versus L-Res treatment). E. Alizarin red staining for the detection of mineral deposition in VSMCs (Scale bar = 50 μm). Five-day vehicle denotes VSMCs cultured in growth medium without stimuli for 5 days.

STAT3, Ac-p53, p53 and p21 were not obvious alterations (Fig. 6C). Also, inhibition of p53 was achieved by using pifithrin-α (PFTα, a p53 inhibitor). Western blotting analysis showed that Ac-p53, p53 as well as p21 maintained lower levels, even the increased levels of p-STAT3 were available owing to activation of IL-6. Furthermore, based on SA-β-Gal staining assay and Alizarin Red S staining analysis, senescence-associated calcification of VSMCs was dramatically inhibited by using the anti-IL-6 neutralization antibody or the p53 inhibitor (Fig. 6D and 6E). These data indicate that senescence-associated calcification of VSMCs is induced by the combined actions of phosphate overload and IL-6 in a p53-dependent manner.

4. Discussion

Cardiovascular calcification, including vascular calcification and valvular calcification, contributes to the high rates of mortality of patients with ESRD (Adeseun et al., 2012; Civilibal et al., 2009; Go et al., 2004a; Nakamura et al., 2009; Nasrallah et al., 2010). Hyperphosphatemia is one the most powerful inducers of cardiovascular calcification in patients with ESRD (Shanahan et al., 2011). In the present study, patients with ESRD showed their higher serum phosphate levels (> 1.45 mM) and IL-6 (≥5.59 pg/ml) compared to those of patients with NDD-CKD. Although the mechanisms are distinct, causes of mineral deposition and calcification are most likely overlapping in both the valve and the vessel.(Civilibal et al., 2009; Johnson et al., 2006) Quantitative evaluation of calcification only based on the plain X-rays and Doppler ultrasound images in this retrospective study, even a number of other non-invasive imaging techniques, such as computed tomography, echocardiography, are available to screen for the presence of cardiovascular calcification (Nitta et al., 2019). Among 60 cases of

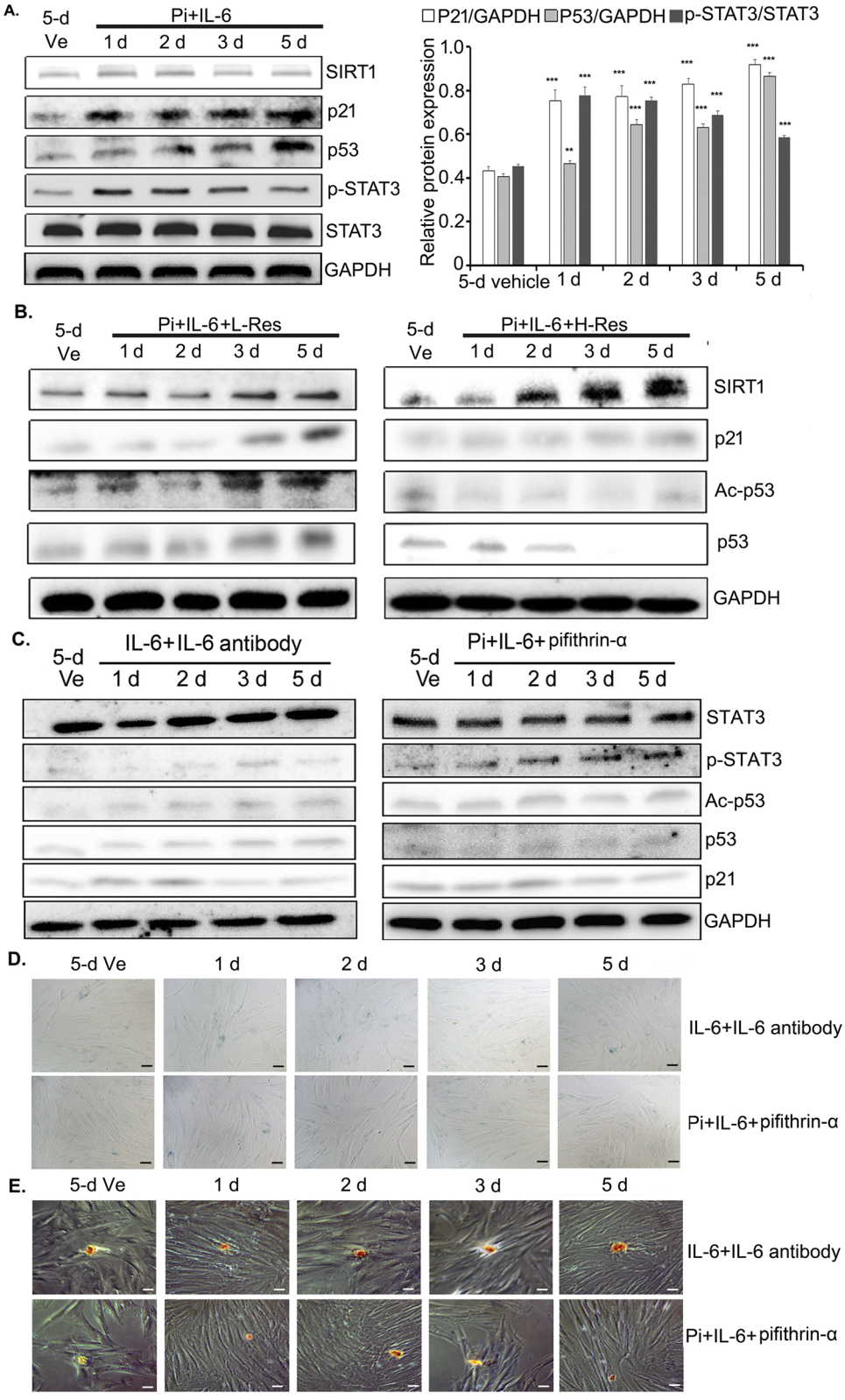

Fig. 6. Aging process is enhanced by the synergistic action of phosphate and IL-6, but inhibited by resveratrol in a dose-dependent manner. A. Western blotting analysis for the detection of p21, SIRT1, p53, STAT3, p-STAT3 in VSMCs treated by both phosphate overload and IL-6. Data were presented as the mean ± SD of triplicate experiments (**$P < 0.01$, ***$P < 0.001$ versus 5-day vehicle). B. Immunoblotting analysis for detection of p21, SIRT1, p53, Ac-p53 in VSMCs exposed to resveratrol, phosphate and IL-6. Five-day vehicle means VSMCs cultured in growth medium without stimuli for 5 days. C. Immunoblotting analysis for detection of p21, p53, Ac-p53, p-STAT3 in VSMCs exposed to the anti-IL-6 antibody as well as IL-6, or to PFTα with both phosphate and IL-6.

ESRD patients with cardiovascular calcification, high levels of serum phosphate were found in 60.00% (36/60) of patients. Therefore, inorganic phosphate may be not a uniquely powerful inducer of calcification.

Although a number of risk factors, such as TNF-α, C-reactive protein and FGF23, have been associated with cardiovascular calcification and mortality in ESRD patients, plasma IL-6 levels in ESRD patients have been shown to predict death better than TNF-α and C-reactive protein concentrations (Zoccali et al., 2006). Importantly, IL-6 is known to be the powerful inducer of cardiovascular calcification in patients with ESRD (Kaminska et al., 2019; Su et al., 2017). We also found that 70.00% of ESRD patients (42/60) had cardiovascular calcification coincident with high levels of serum IL-6. Furthermore, among 56 cases of ESRD patients with both high levels of phosphate and elevated serum

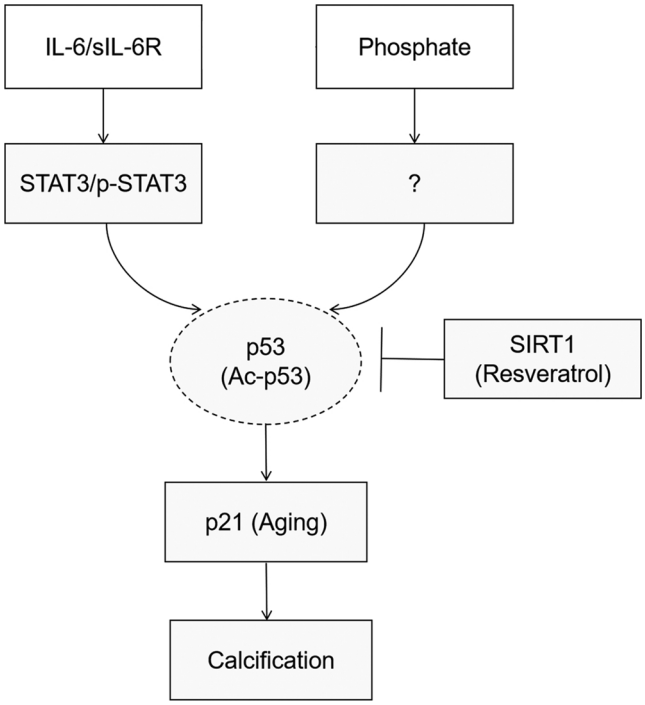

Fig. 7. Schematic diagram of signaling pathway for phosphate and IL-6 inducing senescence-associated calcification in VSMCs.

IL-6, almost half of patients displayed cardiovascular calcification. Our data at least demonstrated that calcification is correlated with high levels of phosphate and elevated serum IL-6 levels in patients with ESRD ($P = 0.00$). Therefore, phosphate overload and IL-6 possibly have synergistic actions in promoting calcification in patients with ESRD.

Both SA-β-Gal and p21 are widely used as the specific markers of senescent cells. Senescence leads to persistent DNA damage and activation of p53/p21, which exerts processes causing growth arrest and senescence.(Kojima et al., 2013) As, well, one of the fundamental features associated with vascular senescence is the crosstalk between inflammation and oxidative stress. A series of reviews and evidences reports that ROS have been found to be increased in aged tissues and can be manipulated in vitro to induce senescence through activation of p53/p21 pathway (Chiou et al., 2018; Johnson et al., 1996; Westin et al., 2011). Downregulation of p21 by RNA interference decreased calcification, suggesting that senescence of VSMCs contributes to vascular calcification (Takemura et al., 2011). Although senescence-associated vascular calcification induced by loading phosphate is well known to be involved in osteoblastic transition of VSMCs,(Yamada et al., 2015) the molecular mechanisms of phosphate-induced senescence of VSMCs remains poorly understood. We found that phosphate overload dramatically increased expression of p21, SA-β-Gal, and p53, coincident with an increased mineral deposition in VSMCs. In addition, higher levels of ROS were successfully detected in VSMCs by exposure to phosphate overload. On the contrary, increasing expression of p21, SA-β-Gal, and p53 was markedly inhibited by resveratrol through SIRT1 activation, coincident with the significantly suppressed levels of ROS. As a member of the sirtuin family of nicotinamide adenine dinucleotide (NAD)-dependent deacetylases, SIRT1 is able to de-acetylate p53 and to promote degradation of p53 (Takemura et al., 2011). Interestingly, phosphate-induced mineral deposition was also attenuated when senescence of VSMCs was blocked by resveratrol. Therefore, p53 plays a critical role in senescence-associated vascular calcification induced by phosphate overload in VSMCs.

The Chronic Renal Insufficiency Cohort study showed that IL-6-induced vascular calcification is a predictor of poor clinical outcome in patients with CKD(Barreto et al., 2010; Pereira et al., 1994; Singh et al., 2016; Su et al., 2017). IL-6 is also a well-known inducer of vascular calcification. According to the present study,(Hénaut and Massy, 2018) to prevent the development or progression of vascular calcification, IL-6 suppression might be one choice of treatment for patients with ESRD. However, no ongoing clinical trial is available that intended to target IL-6 with the goal of decreasing vascular calcification in patients with ESRD due to the risk of complications caused by immunosuppression (Hénaut and Massy, 2018; Ridker et al., 2017). Considering that IL-6/sIL-6R induces premature senescence in human primary fibroblasts depending upon a critical axis of IL-6/sIL-6R/STAT3, and that p53 is essential for the IL-6/sIL-6R-induced premature senescence (Kojima et al., 2013), we were interested in the roles of the IL-6/sIL-6R/STAT3/p53 pathway in the process of senescence-associated vascular calcification in VSMCs. As expected, IL-6 dramatically increased expression of p53, SA-β-Gal, and p21 through activation of STAT3, accompanied by an increased mineral deposition in VSMCs. As there is a potential p-STAT3 binding site (5′-TTnnnnGA-3′) in the *p53* promoter region, luciferase analysis further confirmed that p53 expression was regulated by activation of STAT3 in the present study. On the other hand, IL-6-induced expression of p21, SA-β-Gal, and p53 was markedly inhibited by resveratrol or the anti-IL-6 neutralization antibody. Also, Ac-p53 dramatically decreased in VSMCs after SIRT1 was activated by resveratrol. Mineral deposition was significantly attenuated in accordance with weakened senescence of VSMCs. Thus, p53 plays a major role in regulating IL-6-induced senescence-associated calcification in VSMCs.

Given that both loading phosphate and high serum IL-6 simultaneously occur in patients with ESRD, we presumed that both phosphate overload and IL-6 may have synergistic roles in inducing senescence-associated vascular calcification in VSMCs. As expected, compared with the time-course expression of p21 and p53 induced by either phosphate overload or IL-6 alone (Fig. 4A), the significantly increased p21 and p53 expression were available with 1-day induction of both phosphate overload and IL-6 (Fig. 6A). In concord with these data, an increased mineral deposition was successfully detected in the senescent VSMCs. Senescence-associated calcification of VSMCs induced by the synergistic action of phosphate and IL-6 was dramatically inhibited by the p53 inhibitors. So, the synergistic action of phosphate and IL-6 contributed to senescence-associated vascular calcification in VSMCs depending upon upregulation of p53 (Fig. 7). In addition, H-Res, not L-Res, dramatically inhibited senescence-associated vascular calcification, which was induced by loading phosphate and IL-6. This is a demonstration that anti-aging agents mitigate senescence-associated vascular calcification in a dose-dependent manner.

Taken together, cardiovascular calcification is associated with high levels of phosphate and elevated serum IL-6 levels in patients with ESRD. Although continued advances in understanding the molecular mechanisms of phosphate-induced senescence, we demonstrated that IL-6 induces senescence of VSMCs through activation of the IL-6/sIL-6R/STAT3/p53/p21 pathway. Of importance, p53 plays a major role in senescence-associated vascular calcification induced by phosphate overload and IL-6 in VSMCs. Senescence-associated vascular calcification of VSMCs in patients with ESRD is enhanced by the synergistic actions of loading phosphate and IL-6 in a p53-dependent manner, and is attenuated by anti-aging agents in a dose-dependent manner. Anti-aging therapies may be in favor of decreasing cardiovascular calcification in patients with ESRD.

Funding

This work was supported by the National Natural Science Foundation of China (81772909).

Disclosure

None.

Acknowledgements

We thank Dr. Huan Li, Dr. Xijun Gong (The Second Affiliated Hospital of AHMU) and Dr. Xiaohu Li (The First Affiliated Hospital of AHMU) for reading the clinical images. We would like to thank Dr. Fushen Zhou (Institute of Dermatology at AHMU) and Dr. Hongchao Yin (Peking Union Medical College, Beijing) for providing primary human skin fibroblasts and EAhy926 cells, respectively.

References

Adeseun, Gbemisola A., Xie, Dawei, Wang, Xin, Joffe, Marshall M., Iii, Emile R.Mohler, Townsend, Raymond R., Budoff, Matthew, Rosas, Sylvia E., 2012. Carotid plaque, carotid intima-media thickness, and coronary calcification equally discriminate prevalent cardiovascular disease in kidney disease. Am. J. Nephrol. 36 (4), 342–347.

Agharazii, M., St-Louis, R., Gautier-Bastien, A., Ung, R.V., Mokas, S., Larivière, R., Richard, D.E., 2015. Inflammatory cytokines and reactive oxygen species as mediators of chronic kidney disease-related vascular calcification. Am. J. Hypertens. (6), 746–755 In Press.

Alaly, Ziyad, Shao, Jian Su, Lai, Chung Fang, Huang, Emily, Cai, Jun, Behrmann, Abraham, Cheng, Su Li, Towler, Dwight A., 2007. Aortic Msx2-Wnt calcification cascade is regulated by TNF-α–Dependent signals in diabetic ldlr−/− mice. Arterioscler. Thromb. Vasc. Biol. 27 (12), 2589–2596.

Barreto, Daniela V., Barreto, Fellype C., Liabeuf, Sophie, Temmar, Mohammed, Lemke, Horst-Dieter, Tribouilloy, Christophe, Choukroun, Gabriel, Vanholder, Raymond, Massy, Ziad A., 2010. Plasma interleukin-6 is independently associated with mortality in both hemodialysis and pre-dialysis patients with chronic kidney disease. Kidney Int. 77 (6), 550–556.

Ben-Porath, I., Weinberg, R.A., 2005. The signals and pathways activating cellular senescence. Int. J. Biochem. Cell Biol. 37 (5), 961–976.

Campisi, J., D'Adda, di Fagagna F., 2007. Cellular senescence: when bad things happen to good cells. Nat. Rev. Mol. Cell Biol. 8 (9), 729–740.

Chiou, C.S., Wu, C.M., Dubey, N.K., Lo, W.C., Tsai, F.C., Tung, T.D.X., Hung, W.C., Hsu, W.C., Chen, W.H., Deng, W.P., 2018. Mechanistic insight into hyaluronic acid and platelet-rich plasma-mediated anti-inflammatory and anti-apoptotic activities in osteoarthritic mice. Aging 10 (12), 4152–4165.

Civilibal, M., Caliskan, S., Kurugoglu, S., Candan, C., Canpolat, N., Sever, L., Kasapcopur, O., Arisoy, N., 2009. Progression of coronary calcification in pediatric chronic kidney disease stage 5. Pediatr. Nephrol. 24 (3), 555–563.

Doulgerakis, D., Moyssakis, I., Kapelios, C.J., Eleftheriadou, I., Chorepsima, S., Michail, S., Tentolouris, N., 2017. Cardiac autonomic neuropathy predicts all-cause and cardiovascular mortality in patients with end-stage renal failure: a 5-Year prospective study. Kidney Int. Rep. 2 (4), 686–694.

Go, A.S., Chertow, G.M., Fan, D., McCulloch, C.E., Hsu, C.Y., 2004a. Chronic kidney disease and the risks of death, cardiovascular events, and hospitalization. N. Engl. J. Med. 351 (13), 1296–1305.

Go, A.S., Chertow, G.M., Fan, D., McCulloch, C.E., Hsu, C.Y., 2004b. Chronic kidney disease and the risks of death, cardiovascular events, and hospitalization. J. Vasc. Surg. 41 (1), 177.

Hénaut, L., Massy, Z.A., 2018. New insights into the key role of interleukin 6 in vascular calcification of chronic kidney disease. Nephrol. Dial. Transplant. 33 (4).

Haydar, A.A., Covic, A., Colhoun, H., Rubens, M., Goldsmith, D.J., 2004. Coronary artery calcification and aortic pulse wave velocity in chronic kidney disease patients. Kidney Int. 65 (5), 1790.

Hirano, Toshio, Ishihara, Katsuhiko, Hibi, Masahiko, 2000. Roles of STAT3 in mediating the cell growth, differentiation and survival signals relayed through the IL-6 family of cytokine receptors. Oncogene 19 (21), 2548–2556.

Hruska, K.A., Mathew, S., Lund, R., Qiu, P., Pratt, R., 2008. Hyperphosphatemia of chronic kidney disease. Kidney Int. 74 (2), 148–157.

Isakova, T., Cai, X., Lee, J., Xie, D., Wang, X., Mehta, R., Allen, N.B., Scialla, J.J., Pencina, M.J., Anderson, A.H., 2018. Longitudinal FGF23 trajectories and mortality in patients with CKD. J. Am. Soc. Nephrol. 29 (2) ASN.2017070772.

Johnson, R.C., Leopold, J.A., Loscalzo, J., 2006. Vascular calcification: pathobiological mechanisms and clinical implications. Circ. Res. 99 (10), 1044.

Johnson, T.M., Yu, Z.X., Ferrans, V.J., Lowenstein, R.A., Finkel, T., 1996. Reactive oxygen species are downstream mediators of p53-dependent apoptosis. Proc. Natl. Acad. Sci. U. S. A. 93 (21), 11848–11852.

Kaminska, J., Stopinski, M., Mucha, K., Jedrzejczak, A., Golebiowski, M., Niewczas, M.A., Paczek, L., Foroncewicz, B., 2019. IL 6 but not TNF is linked to coronary artery calcification in patients with chronic kidney disease. Cytokine 120, 9–14.

Kojima, H., Inoue, T., Kunimoto, H., Nakajima, K., 2013. IL-6-STAT3 signaling and premature senescence. Jak-Stat. 2 (4), e25763.

Kojima, H., Kunimoto, H., Inoue, T., Nakajima, K., 2012. The STAT3-IGFBP5 axis is critical for IL-6/gp130-induced premature senescence in human fibroblasts. Cell Cycle 11 (4), 730–739.

Kuroo, Makoto, Matsumura, Yutaka, Aizawa, Hiroki, Kawaguchi, Hiroshi, Suga, Tatsuo, Utsugi, Toshihiro, Ohyama, Yoshio, Kurabayashi, Masahiko, Kaname, Tadashi, Kume, Eisuke, 1997. Mutation of the mouse klotho gene leads to a syndrome resembling ageing. Nature 390 (6655), 45–51.

Kurosu, H., Yamamoto, M., Clark, J.D., Pastor, J.V., Nandi, A., Gurnani, P., Mcguinness, O.P., Chikuda, H., Yamaguchi, M., Kawaguchi, H., 2005. Suppression of aging in mice by the hormone Klotho. Science 309 (5742), 1829–1833.

London, G.M., Guerin, A.P., Marchais, S.J., Metivier, F., Pannier, B., Adda, H., 2003. Arterial media calcification in end-stage renal disease: impact on all-cause and cardiovascular mortality. Nephrol. Dial. Transplant. 18 (9), 1731–1740.

Nakamura, S., Ishibashi-Ueda, H., Niizuma, S., Yoshihara, F., Horio, T., Kawano, Y., 2009. Coronary calcification in patients with chronic kidney disease and coronary artery disease. Clin. J. Am. Soc. Nephrol. 4 (12), 1892–1900.

Nakano-Kurimoto, R., Ikeda, K., Uraoka, M., Nakagawa, Y., Yutaka, K., Koide, M., Takahashi, T., Matoba, S., Yamada, H., Okigaki, M., 2009. Replicative senescence of vascular smooth muscle cells enhances the calcification through initiating the osteoblastic transition. Am. J. Physiol. Heart Circ. Physiol. 297 (5), H1673.

Nasrallah, M.M., Elshehaby, A.R., Salem, M.M., Osman, N.A., El, Sheikh E., Ua, Sharaf El Din, 2010. Fibroblast growth factor-23 (FGF-23) is independently correlated to aortic calcification in haemodialysis patients. Nephrol. Dial. Transplant. 25 (8), 2679–2685.

Nitta, K., Ogawa, T., Hanafusa, N., Tsuchiya, K., 2019. Recent advances in the management of vascular calcification in patients with end-stage renal disease. Contrib. Nephrol. 198, 62–72.

O'Neill, W.C., 2016. Targeting serum calcium in chronic kidney disease and end-stage renal disease: is normal too high? Kidney Int. 89 (1), 40–45.

Pereira, B.J., Shapiro, L., King, A.J., Falagas, M.E., Strom, J.A., Dinarello, C.A., 1994. Plasma levels of IL-1 beta, TNF alpha and their specific inhibitors in undialyzed chronic renal failure, CAPD and hemodialysis patients. Kidney Int. 45 (3), 890.

Quarles, L.Darryl, 2008. Endocrine functions of bone in mineral metabolism regulation. J. Clin. Invest. 118 (12), 3820.

Razzaque, M.S., Sitara, D., Taguchi, T., Starnaud, R., Lanske, B., 2006. Premature aging-like phenotype in fibroblast growth factor 23 null mice is a vitamin D mediated process. FASEB J. 20 (6), 720–722.

Ridker, P.M., Everett, B.M., Thuren, T., Macfadyen, J.G., Chang, W.H., Ballantyne, C., Fonseca, F., Nicolau, J., Koenig, W., Anker, S.D., 2017. Antiinflammatory therapy with Canakinumab for atherosclerotic disease. N. Engl. J. Med. 377 (12), 1119.

Shanahan, Catherine M., Crouthamel, Matthew H., Kapustin, Alexander, Giachelli, Cecilia M., 2011. Arterial calcification in chronic kidney disease: key roles for calcium and phosphate. Circ. Res. 109 (6), 697–711.

Shioi, Atsushi, Katagi, Miwako, Okuno, Yasuhisa, Mori, Katsuhito, Jono, Shuichi, Koyama, Hidenori, Nishizawa, Yoshiki, 2002. Induction of bone-type alkaline phosphatase in human vascular smooth muscle cells roles of tumor necrosis Factor-α and oncostatin m derived from macrophages. Circ. Res. 91 (1), 9–16.

Singh, S., Grabner, A., Yanucil, C., Schramm, K., Czaya, B., Krick, S., Czaja, M.J., Bartz, R., Abraham, R., Di Marco, G.S., Brand, M., Wolf, M., Faul, C., 2016. Fibroblast growth factor 23 directly targets hepatocytes to promote inflammation in chronic kidney disease. Kidney Int. 90 (5), 985–996.

Smith, E.R., 2016. Vascular calcification in Uremia: new-age concepts about an old-age problem. Methods Mol. Biol. 1397, 175–208.

Stompór, T., Rajzer, M., Kaweckajaszcz, K., Dembińskakieć, A., Janda, K., Wójcik, K., Tabor, B., Zdzienicka, A., Grzybowska, E.J., Sulowicz, W., 2005. Renal transplantation ameliorates the progression of arterial stiffness in patients treated with peritoneal dialysis. Perit. Dial. Int. 25 (5), 492–496.

Stompor, T.P., Pasowicz, M., Sulowicz, W., Dembinska-Kiec, A., Janda, K., Wojcik, K., Tracz, W., Zdzienicka, A., Konieczynska, M., Klimeczek, P., Janusz-Grzybowska, E., 2004. Trends and dynamics of changes in calcification score over the 1-year observation period in patients on peritoneal dialysis. Am. J. Kidney Dis. 44 (3), 517–528.

Su, Hua, Lei, Chun Tao, Zhang, Chun, 2017. Interleukin-6 signaling pathway and its role in kidney disease: an update. Front. Immunol. 8.

Takemura, A., Iijima, K., Ota, H., Son, B.K., Ito, Y., Ogawa, S., Eto, M., Akishita, M., Ouchi, Y., 2011. Sirtuin 1 retards hyperphosphatemia-induced calcification of vascular smooth muscle cells. Arterioscler. Thromb. Vasc. Biol. 31 (9), 2054.

Tu, Z., Zhang, S., Zhou, G., Zhou, L., Xiang, Q., Chen, Q., Zhao, P., Zhan, H., Zhou, H., Sun, L., 2018. LMO4 is a disease-provocative transcription coregulator activated by IL-23 in psoriatic keratinocytes. J. Invest. Dermatol. 138 (5), 1078–1087.

Westin, E.R., Aykin-Burns, N., Buckingham, E.M., Spitz, D.R., Goldman, F.D., Klingelhutz, A.J., 2011. The p53/p21(WAF/CIP) pathway mediates oxidative stress and senescence in dyskeratosis congenita cells with telomerase insufficiency. Antioxid. Redox Signal. 14 (6), 985–997.

Yamada, S., Tatsumoto, N., Tokumoto, M., Noguchi, H., Ooboshi, H., Kitazono, T., Tsuruya, K., 2015. Phosphate binders prevent phosphate-induced cellular senescence of vascular smooth muscle cells and vascular calcification in a modified, adenine-based uremic rat model. Calcif. Tissue Int. 96 (4), 347–358.

Yin, Tintut, Patel, Jignesh, Parhami, Farhad, Demer, Linda L., 2000. Tumor necrosis Factor-α promotes in vitro calcification of vascular cells via the cAMP pathway. Circulation 102 (21), 2636–2642.

Zhao, P., Guo, S., Tu, Z., Di, L., Zha, X., Zhou, H., Zhang, X., 2016. Grhl3 induces human epithelial tumor cell migration and invasion via downregulation of E-cadherin. Acta Biochim. Biophys. Sin. 48 (3), 266–274.

Zoccali, C., Tripepi, G., Mallamaci, F., 2006. Dissecting inflammation in ESRD: do cytokines and C-reactive protein have a complementary prognostic value for mortality in dialysis patients? J. Am. Soc. Nephrol. 17 (12 Suppl 3), S169–173.